We are IntechOpen, the world's leading publisher of Open Access books
Built by scientists, for scientists

6,900
Open access books available

186,000
International authors and editors

200M
Downloads

Our authors are among the

154
Countries delivered to

TOP 1%
most cited scientists

12.2%
Contributors from top 500 universities

CLARIVATE ANALYTICS
BOOK CITATION INDEX
INDEXED

WEB OF SCIENCE™

Selection of our books indexed in the Book Citation Index
in Web of Science™ Core Collection (BKCI)

Interested in publishing with us?
Contact book.department@intechopen.com

Numbers displayed above are based on latest data collected.
For more information visit www.intechopen.com

In Search of Optimal Laser Settings for Lithotripsy by Numerical Response Surfaces of Ablation and Retropulsion

Jian J. Zhang

Abstract

Even though ureteroscopic laser lithotripsy (URSL) has become the preferred treatment option for urolithiasis due to shorter operation time and a better stone-free rate, the optimum laser pulse settings for URSL with the shortest operative times remain unknown. In this chapter, two sets of design of experiments (DOE) were conducted with response surface methodology: 1) the quantitative responses of calculus ablation and retropulsion in terms of the pulse energy, pulse width, and the number of pulses of a prototype Chromium (Cr3+), Thulium (Tm3+), Holmium (Ho3+) triple doped yttrium aluminum garnet (CTH:YAG) laser system. The ablation or retropulsion is inversely proportional to the pulse width, and the pulse width has a higher impact coefficient for the ablation than for the retropulsion. The quadratic fit of the response surface for the volume of ablation has a nonlinear relationship with the pulse width and number of pulses. 2) the laser setting optimization of laser lithotripsy of a commercially available CTH: YAG laser system. The experimental setup is based on a benchtop model first introduced by Sroka's group. Comparing to frequency, the laser pulse energy or peak power has a higher impact coefficient to stone retropulsion as compared to stone ablation in CTH: YAG laser lithotripsy. The most efficient way to curtail stone retropulsion during laser lithotripsy is to lower the laser pulse peak power.

Keywords: stone, ablation, lithotripsy, retropulsion, response surface, design of experiment, pulse energy, peak power

1. Introduction

Urolithiasis, which is hard tissue (stone) formation in the urinary tract due to supersaturated body fluids, has risen steadily in recent decades. The leading causes of stone formation are the reduction of urine volume (or water intake), an increased calcium oxalate/calcium phosphate secretion, urine pH alteration, or urinary tract infections (urease forming bacteria) [1–4]. The prevalence in western countries is estimated at 10%-15%, and the recurrence rate is averaging up to 50% [5–7]. And according to Charles D. Scales [8], the prevalence of kidney stones nearly doubled in about 17 years from ~1995 to 2012. The prevalence of urolithiasis has been rising internationally over recent decades because of population growth, predicted obesity

trends, and estimated increases in diabetes, just to name a few. The annual treatment cost of stone disease could reach >\$5 billion/yr. (in 2014 prices) in the United States by the year 2030 [9, 10].

Shockwave lithotripsy (SWL) and ureteroscopic laser lithotripsy (URSL) are the most commonly performed procedures in the United States for the treatment of patients with urinary calculi [11, 12]. URSL is now the preferred treatment option for urolithiasis due to relatively shorter operative time and a better stone-free rate [1].

The first laser device was invented in 1960 by Maiman [13] based on the theoretical work by Townes and Schawlow. And in 1968, Mulvaney et al. [14] reported the first fragmentation of kidney stones with a pulsed ruby laser (λ: 694 nm) in an in vitro experiment by using quartz rods to deliver the laser light to the treatment site. Since then, a few laser lithotripters were clinically available, including the pulsed-dye laser, the frequency-doubled pulsed Neodymium ($Nd3+$) doped Yttrium aluminum garnet (Nd:YAG) laser (FREDDY), and the Ho: YAG laser [15–17]. The Ho: YAG laser with relatively long-pulse is the most effective and adaptable tool for lithotripsy among all the lasers comparing to nanosecond Nd: YAG lasers. It can disintegrate all kinds of calculus and provoke less calculus retropulsion during procedure than the short-pulsed lasers [18–22]. Since soon after its debut in the 1990s, the Ho: YAG laser has been the preferred lithotripter for the therapy of urinary calculus. It is a solid-state pulsed laser at a wavelength of 2.13 μm. This wavelength is easily absorbed by water (~26 cm^{-1} [23]), providing a wide safety margin for lithotripsy in the urinary tract [24–26]. Aside from treating calculi, it can be used for soft tissue applications such as treating urinary strictures and ablating urothelial tumors. The high-powered variant can also be used for the enucleation of the prostate (HoLEP). Recently, another technology has been explored for the next generation laser lithotripsy: the Thulium fiber laser [27, 28]. This promising technology offers several advantages that may expand the boundaries of laser lithotripsy [28, 29].

The dominant mechanism in Ho: YAG laser lithotripsy is photothermal along with minor effects of acoustic emission [29]. Because the Ho: YAG laser's thermal diffusion time in the water over the optical penetration depth is 286 ms [30], which is well above the laser pulse width (less than a few milliseconds, mostly in the 100 s of μs), in other words, it is photo-thermally confined. And the laser is not photo-mechanical or stress confined in water since the acoustic diffusion time over the optical penetration depth is 0.267 μs, much less than the Ho: YAG laser pulse width. The water has a strong absorption at the Ho: YAG 2.1 μm wavelength and the calculus ablation was dependent on the water content in calculus phantom [31, 32]. The temperature of the illuminated area of the urinary calculi due to the direct laser photon absorption raises above the ablation threshold, subsequently creating the expulsion of fractured crack-up pieces. Furthermore, the absorption of the laser photon by the liquid between the fiber end and calculus produces a vapor bubble, and the crashing of the bubble generates shockwave. The bubble should not be called the "cavitation" bubble as it does in [30, 33] because cavitation is a phenomenon in which rapid changes of pressure in a liquid lead to the formation of small vapor-filled cavities in places where the pressure is relatively low, while during laser lithotripsy, the bubble is generated by heated water vapor with relatively high pressure. This vapor bubble usually has a minimal mechanical effect on hard tissues but rather parts the water (the "Moses effect" [34]) for direct delivery of the remaining part of the laser light onto the stone [35]. The term "Moses effect" technology is also used by breaking one laser pulse into two, where the first pulse generates a bubble between the fiber tip and the stone to let the second pulse through this bubble to the surface of the stone [36]. The shock-wave image can be captured by a high-speed camera with ~1 μs frame interval [37]; it is a disturbance wave that is faster than the sound wave, which can quickly damp down to sound wave speed [38].

During laser-calculus interaction, the urinary calculus is subject to retropulsion forces caused by the combined effects of ablated particle ejection, interstitial water vaporization, and bubble expansion/collapse [39–41]. And an asymmetric collapse of the bubble near a solid boundary can generate a water jet in the time scale of milliseconds [30]. Therefore, because of the recoil momentum, the calculus is moved away from the end of the laser fiber. The calculus motion prolongs the procedure time because of the burdensome procedure needed to reorient the laser fiber to the new calculus locality. Earlier retropulsion studies quantified calculus retropulsion distance by altering laser pulse energy, pulse frequency, and fiber core size [42–44]. Retropulsion boosted with the laser pulse energy and the laser fiber core size. Moreover, Charles D. Scales et al. reported that a longer pulse width reduced calculus retropulsion distance during a procedure without diminishing ablation efficiency significantly [45].

Although laser lithotripsy is now the preferred treatment option for urolithiasis because it is capable of fragmenting calculus of all known composition, including hard calcium oxalate monohydrate, brushite, and cystine calculus [22, 24, 25, 29], and the rising prevalence of calculus disease has led to similarly increasing efforts to optimize ureteroscopic treatment [43, 45–52], the operative time for the stone procedure can be well above the one hour mark. According to Levi A. Deters et al. [53], URSL management of renal stones and ureteral stones were markedly different, with a significant increase in operative time (60% more) for renal stones and a significant lower stone-free rate (27% lower). And of the 213 cases, the average operative time for the renal group (98 cases) is 112 min and range up to 245 min, and the average operative time for the ureteral group (115 cases) is 70 min and range up to 185 min.

The response surface methodology (RSM) is a powerful statistical tool that can generate the numerical relationship between some key performance variables (responses) and device control parameters (control inputs). Although the model is only an approximation most of the time because of limited knowledge of the process, the RSM plus design of experiments (DOE) can produce analytical models (equations) that can depict 1) the relative impact of the control inputs on the responses by comparing their coefficients in the coded equations; 2) optimization of the responses with proper control inputs.

In this chapter, two sets of DOE experiments were conducted with response surface methodology: 1) the quantitative responses of calculus ablation and retropulsion in terms of the pulse energy, pulse width, and the number of pulses of a prototype CTH: YAG laser system. This step is to understand the dominant laser parameters that control the lithotripsy outcome, so that preferred laser settings can be derived for the next generation of laser lithotripter; 2) the laser setting optimization of laser lithotripsy of a commercially available CTH: YAG laser system. This experiment is to identify a series of laser settings for relatively efficient laser lithotripsy in terms of laser pulse energy and peak power.

2. Experimental method and setup

2.1 The quantitative responses of calculus ablation and retropulsion in terms of the pulse energy, pulse width, and the number of pulses of a prototype CTH: YAG laser system

In this study, the key components of the setup of the experimental materials are listed in **Table 1**.

A prototype CTH:YAG laser had pulse energy from 0.2 J to 3.0 J with variable pulse width from 150 μs to 1000 μs at 2.13 μm. This range of pulse duration is

Item	Description
Laser	Prototype laser
Fiber	365-μm Core (S-LLF365 SureFlex Fiber, American Medical Systems, San Jose, CA, USA)
Phantom	White gypsum cement UtralCal®30 (United States Gypsum Company, Chicago, IL) [54]
Camera	Photron Fastcam SA5 (Photron USA, Inc. San Diego, CA)
Digital microscope	VHX-900F (Keyence, Elmwood Park, NJ, USA)
Program	Design-Expert® (Stat-Ease, Inc., Minneapolis, MN 55413)

Table 1.
The list of components of the experimental setup.

known to generate a photothermal effect to fragment the calculus [51]. Each data point is the average of 10 sample measurements.

Figure 1 is the pictures of the test setup, (a) ablation test setup, and (b) retropulsion test setup. In the ablation test setup (a) submerged in the distilled water, the fiber was held vertically by a clamp with its tip in contact with the calculus phantom underneath the fiber inside a holder. The stone was held fixed during the ablation study.

The laser ablation crater volume in the phantom due to the laser pulse and calculus interaction was measured by a digital microscope (VHX-900F, Keyence, Elmwood Park, NJ, USA). In the retropulsion test setup (b), the fiber was held horizontally, pointing to an underwater pendulum phantom cube with a dimension of $10 \times 10 \times 10$ mm3. The pendulum length was ~200 mm, and the phantom was held by 2 strings with a separation of ~10 mm in a clear plastic basket. The retropulsion motion of the calculus phantom was recorded and analyzed by a high-speed camera.

Figure 2 is a screenshot of DOE by Design-Expert®10. There are three categories of the laser parameter settings: energy, number of pulses, and electrical pump pulse widths (not the optical output pulse width). The ten-pulses range was selected since the typical retropulsion of a $10 \times 10 \times 10$ mm3 will reach its maximum amplitude after ~1 s of 10 Hz 1 J pulse train from the fiber tip [52]. There are $5 \times 3 \times 3 = 45$ data points with the combination of all the laser parameters.

2.2 The laser setting optimization of laser lithotripsy of a commercially available CTH:YAG laser system

It is challenging to characterizing the URSL performance (ablation and retropulsion) in one setup that can mimic the clinical situation, especially measuring retropulsion [55–61]. In this study, in vitro investigations of Ho:YAG laser-induced stone ablation and retropulsion were performed with a benchtop model first introduced by Sroka's group [55, 60]. It is a test that can be performed in a highly reproducible manner using a hands-free setup and measuring the effects of multiple pulses which are mimicking the clinical situation. The advantage of this setup has two folds: 1) No human factor, hands-free, independent repetitive experiments; 2) Providing measurement results for both ablation rate and retropulsion speed. Although the stone moves during the test, which means the distance between the fiber tip and the stone is not a constant, which will report a lower ablation rate, it is still an efficient way to generate meaningful data in terms of ablation and retropulsion for comparing different laser modes. **Table 2** is a description of the list of the key components of the setup.
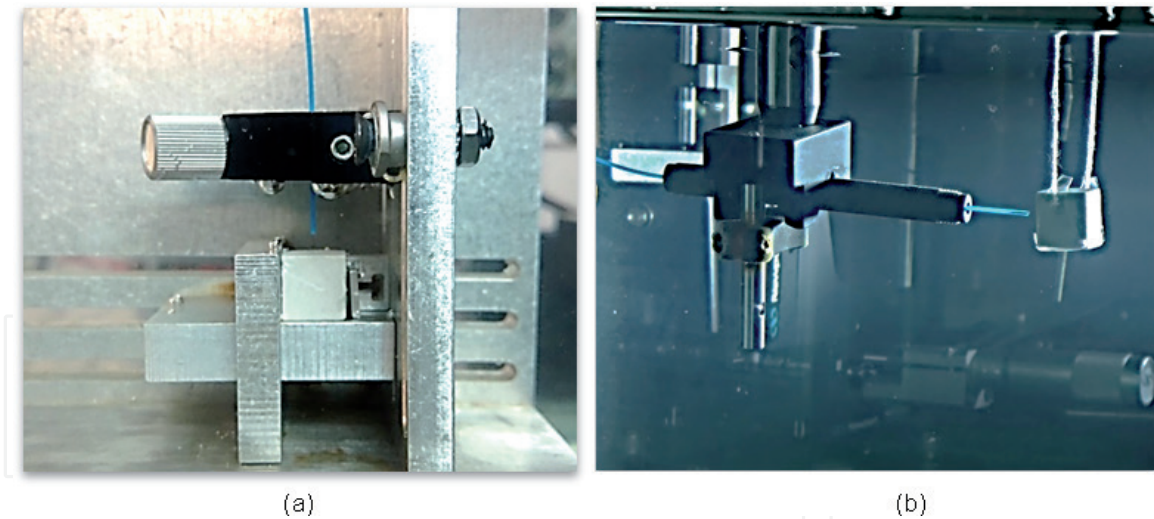
Figure 1.
The pictures of the test setup, (a) ablation test setup with 10 mm phantom; (b) Retropulsion test setup with 10 mm phantom.

Select	Std	Run	Factor 1 A:Number of...	Factor 2 B:Energy J	Factor 3 C:Pulse width us
	13	1	3.00	3.00	1000.00
	14	2	10.00	3.00	1000.00
	12	3	1.00	1.00	1000.00
	1	4	1.00	0.20	333.00
	4	5	3.00	2.00	333.00
	11	6	10.00	0.20	1000.00
	6	7	10.00	3.00	333.00
	3	8	3.00	2.00	333.00
	10	9	1.00	3.00	667.00
	5	10	1.00	3.00	333.00
	9	11	10.00	2.00	667.00
	8	12	3.00	0.20	667.00
	2	13	10.00	0.20	333.00
	7	14	3.00	0.20	667.00

Figure 2.
A screenshot of DOE by DesignExpert-10.

The setup, an acrylic cylinder with a drill hole mimicking the ureter ending in a conical base, is illustrated in **Figure 3**. The diameter of the drill hole can be adapted to the clinical situation (e.g., ureter diameter) or stone size. The stone phantom is a 5 mm cubic shape Bego stone with a composition of 15:3 [62]. The setup is in an upright position filled with the saline at a designated flow speed. The optical fiber is attached through a borehole at the base of the acrylic cylinder. Therefore, laser energy can be delivered to the stone phantom to produce vertical displacement. The gravity and the viscosity of the water are the steady resistances to this motion.

The ablation is quantified by the stone phantom mass deficit after the laser stone interaction by a scale with a resolution of +/− 0.0001 g (Entris 224-1S Sartorius Lab Instruments GmbH & Co. KG, Goettingen, Germany).

The retropulsion is quantified by the vertical displacement velocity of the stone during the laser stone interaction. A high-speed camera, Sony RX100 IV (1000 fps), oriented perpendicular to the upright motion and aimed to the middle of the artificial ureter, registers the event for ~7 seconds. The video subsequently is analyzed in MATLAB, and a representative stone sample vertical displacement graph vs. video frame is illustrated in **Figure 3(B)**. Initial data assessment incorporates background rectification and color tracking algorithm, recognition of the

Item	Description
Laser	PowerSuite™ Ho:YAG 100 W (VersaPulse® 100 W, Lumenis Ltd., Yokneam, Israel)
Fiber	365-µm Core (S-LLF365 SureFlex Fiber, American Medical Systems, San Jose, CA, USA)
Phantom	BEGO Stone 15:3 (BEGO GmbH & Co. KG, Bremen, Germany)
Camera	Sony RX100 IV (Sony Corporation of America, NY, USA)
Balance	Sartorius Entris 224-1S (Sartorius Lab Instruments GmbH & Co. KG, Goettingen, Germany)
Program	Design-Expert® (Stat-Ease, Inc., Minneapolis, MN 55413)

Table 2.
*The list of components of the experimental setup.*

(A)   (B)
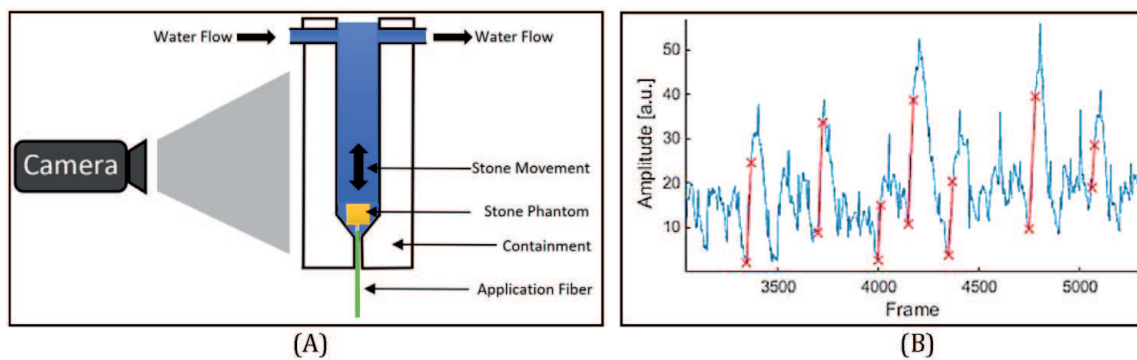
Figure 3.
(A) Test setup including the stone phantom containment vessel, the water flow inlet, and outlet tubes, application fiber, and a high-speed camera. (B) Stone phantom vertical movement vs. video frame.


(A)   **(B)**
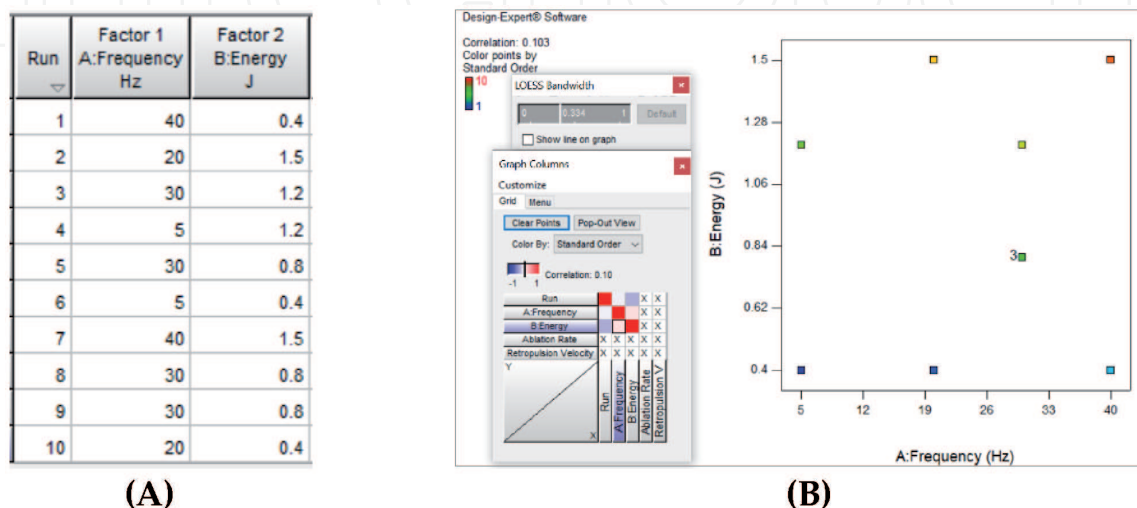
Figure 4.
A few screen shots of the DOE. (A) Design layout; (B) design graphic columns.

center of weight of the traced stone image in each frame and tracing the center of weight position as a function of time. Afterwards, each rising wing can be utilized to obtain the ascending vertical speed. The 1st Derivative of rising flanks displays the mean velocity of the stone $v = \partial x/\partial t$ (x-displacement, t-time), and the velocity of rising flanks is proportional to the applied momentum $p = m * v$ (m-stone mass, v-stone velocity).

The experiment is designed by Design-Expert® with randomized optimal (custom), two replicate points, and two lack-of-fit points. **Figure 4** is a few screenshots of the DOE of laser pulse energy: 0.2, 0.4, 0.6, 0.8, 1.2, 1.5 J and frequency: 5, 10, 15, 20, 30, 40 Hz. A sample size of 14 is used for each data point, and each sample was applied with 15 seconds long laser dose.

3. Results

3.1 The quantitative responses of calculus ablation and retropulsion in terms of the pulse energy, pulse width, and the number of pulses of a prototype CTH:YAG laser system

3.1.1 Retropulsion amplitude data

The retropulsion videos taken by a high-speed camera at 10 k FPS were analyzed by a MATLAB program for the pendulum swing amplitude. **Figure 5(a)** is some sample curves of the retropulsion movement; each data point is the average of 10 measurements.
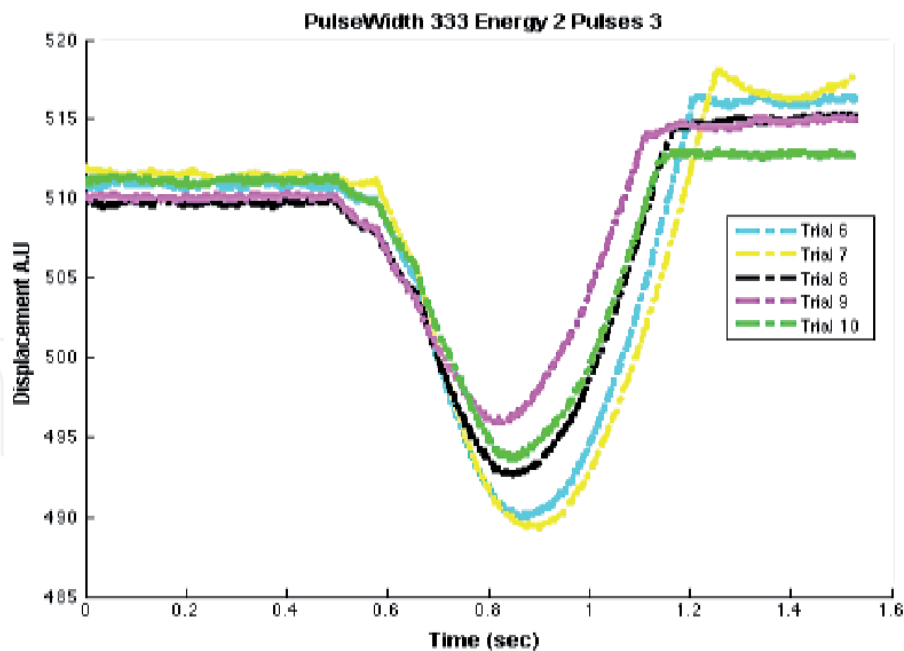

Figure 5.
Retropulsion amplitude measurement results.

4. Retropulsion amplitude response surface

Figure 6 is the screenshots of the response surface of retropulsion amplitude at the pulse energy level of (a) 1 J; (b) 2 J; (c) 3 J. The analytical formula of the response surface of retropulsion is shown in Formula (1). The ANOVA shows
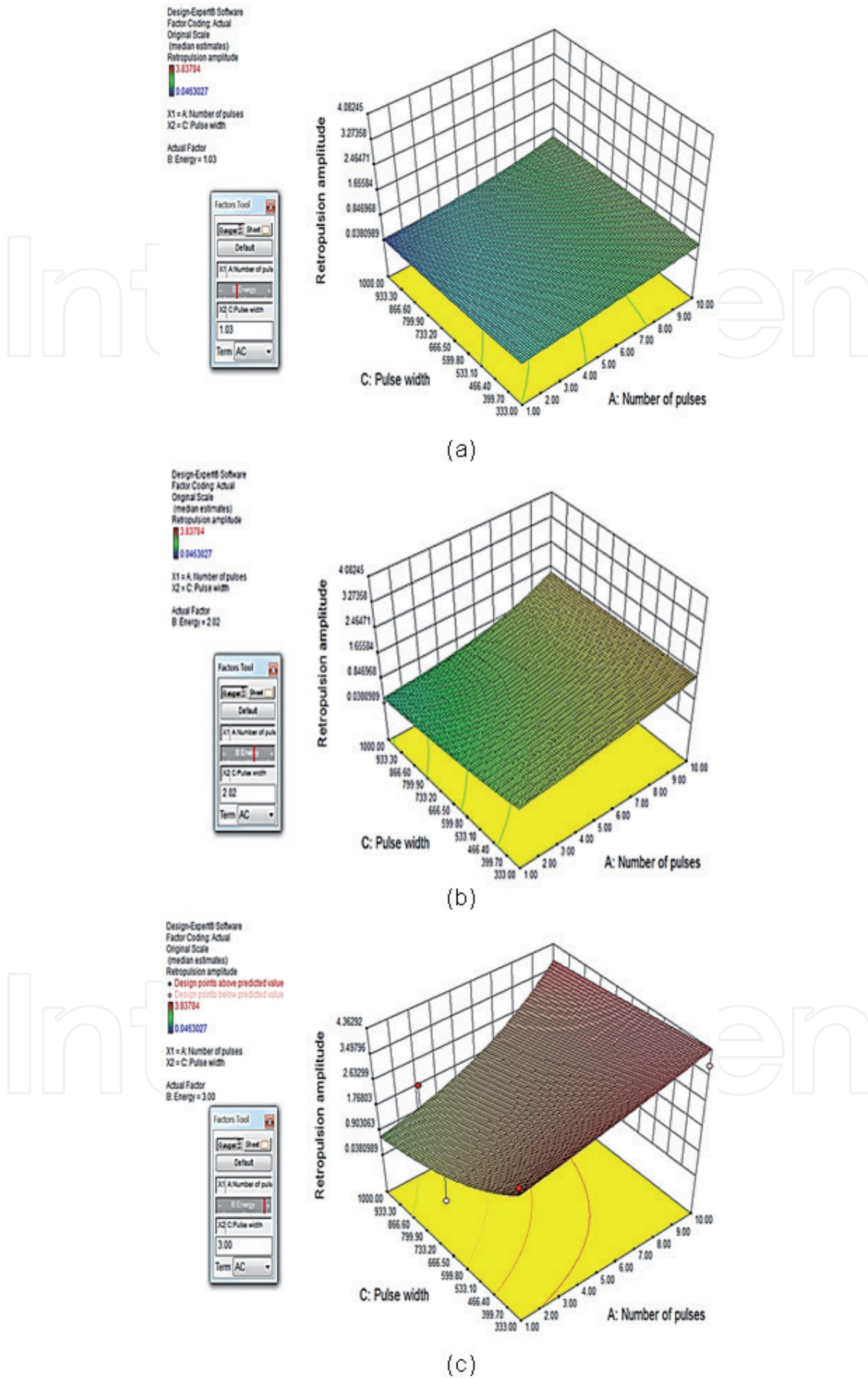
Figure 6.
The screen shots of the response surface of retropulsion amplitude against pulse width and number of pulses at pulse energy level of (a) 1 J; (b) 2 J; (c) 3 J.

an insignificant lack of fit, acceptable agreement of the Predicted and Adjusted R-Squares, and acceptable precision (8.324, > 4.0).

$$\text{Ln}(A) = 0.56 + 0.08n + 1.42\varepsilon - 0.0021\tau - 0.039n\varepsilon + 0.00022n\tau - 0.00011\varepsilon\tau \qquad (1)$$

Where A is the amplitude of retropulsion in mm, n is the pulse number, ε is the pulse energy in J, and τ is the pulse width in μs.

5. Volume of ablation data

The volume of the hole by laser ablation was quantified by a digital microscope. A representative picture is in **Figure 7**.
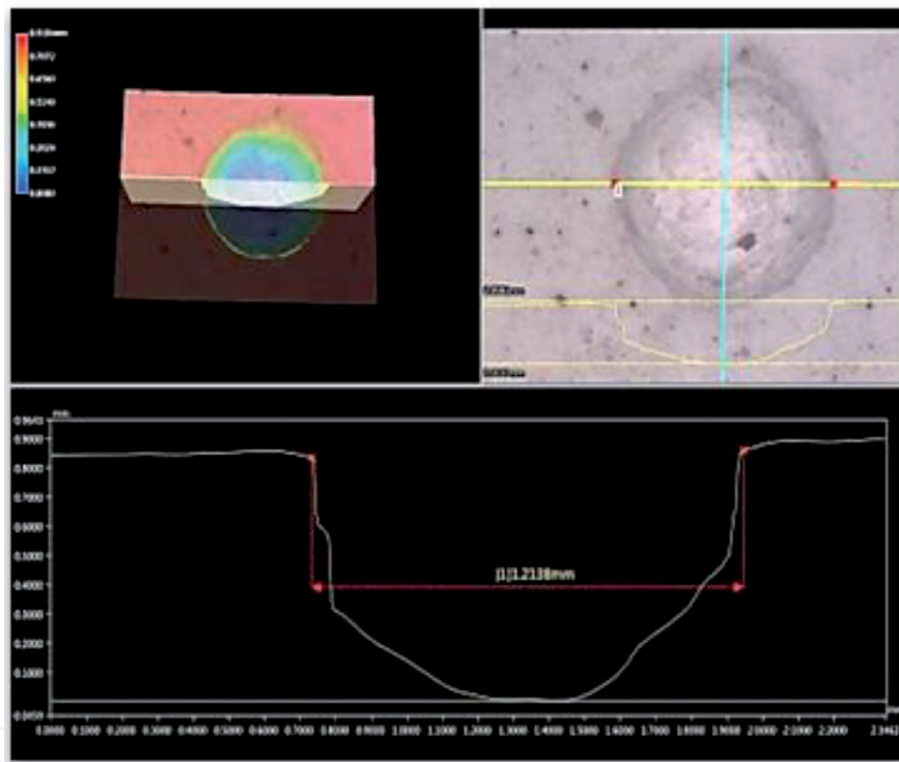
Figure 7.
Volume of ablation response measurement results. Screenshot of VHX-900F digital microscope;

6. Volume of ablation response surface

According to the response surface information from the above section, the Design-Expert® -10 app can produce a response surface and the analytical equation. **Figure 8** is the pictures of the response surface of volume of ablation versus the pulse width and the number of pulses at the pulse energy status of (a) 1 J; (b) 2 J; (c) 3 J. The analytical formula of the response surface of the volume of ablation, including the polynomial terms of two factors interactions, is shown in Formula (2). The ANOVA shows an insignificant lack of fit, acceptable agreement of the Predicted (0.8636) and Adjusted (0.9177) R-Squares, and acceptable precision (15.46, > 4.0).

$$Ln(V) = -0.27 + 0.023n + 1.11\varepsilon - 0.0083\tau + 0.011n\varepsilon + 0.00047n\tau + 0.0012\varepsilon\tau \quad (2)$$

Where V is the ablation volume in mm^3, n is the pulse number, ε is the pulse energy in J, and τ is the pulse width in µs.

Figure 9 is the pictures of the response surface of ablation volume under the quadratic fit with pulse width and the number of pulses at the pulse energy status of (a) 1 J; (b) 2 J; (c) 3 J. The analytical equation of the response surface of ablation volume, involving the polynomial terms of two factors interactions, is illustrated in Eq. (3). The ANOVA shows an insignificant lack of fit, acceptable agreement of the Predicted (0.9900) and Adjusted (0.9999) R-Squares, and acceptable precision (466.6, > 4.0).

$$Ln(V) = -1.16 + 0.94n + 3.46\varepsilon - 0.021\tau + 0.0031n\varepsilon + 0.00048n\tau +$$
$$0.0014\varepsilon\tau - 0.078n^2 - 0.77\varepsilon^2 + 0.0000093\tau^2 \quad (3)$$

Where V is the ablation volume in mm^3, n is the pulse number, ε is the pulse energy in J, and τ is the pulse width in µs.

Figure 10 is the ablation and retropulsion in percentages by 10 pulses of the 1000 µs pulses versus those of 333 µs. The variation of the volume of between long and short pulse is comparatively larger at 1 J and 2 J level contrasting to retropulsion. Namely, ablation declines more swiftly than retropulsion when expanding pulse width.

6.1 The laser setting optimization of laser lithotripsy of a commercially available CTH:YAG laser system

6.1.1 Response surface in terms of laser pulse energy

Figure 11(A) and **(B)** are the screenshots of the response surface of ablation rate and the retropulsion velocity; each data point is the average of 14 measurements. The ANOVA shows an insignificant lack of fit (except P = 0.04 for the ablation rate), acceptable agreement of the predicted and adjusted R-squares, and acceptable precision (> 4.0).

The coded equation can predict the response for each of the control parameters. By convention, the high elevations of the parameters are coded as +1, and the low elevations of the parameters are coded as −1. The coded equation is valuable at attaining the comparable impact parameters by the coefficients of each term.

Coded analytical equation of ablation and retropulsion by laser pulse energy is:

$$A_{P-100}{}^{0.5} = 0.50 + 0.34A + 0.49B + 0.18AB \quad (4)$$

$$R_{P-100} = 92.69 + 4.94A + 28.47B \quad (5)$$

A_{P-100} – Ablation rate, R_{P-100} -Retropulsion velocity, A-Frequency, B-Energy

From the coded equation, we can see the impact of the laser pulse energy is 1.4 times that of the frequency on the ablation rate, while for retropulsion velocity, the impact of the laser pulse energy is 5.8 times that of the frequency. This indicates the laser pulse energy setting has a vital impact on both ablation rate and retropulsion velocity.
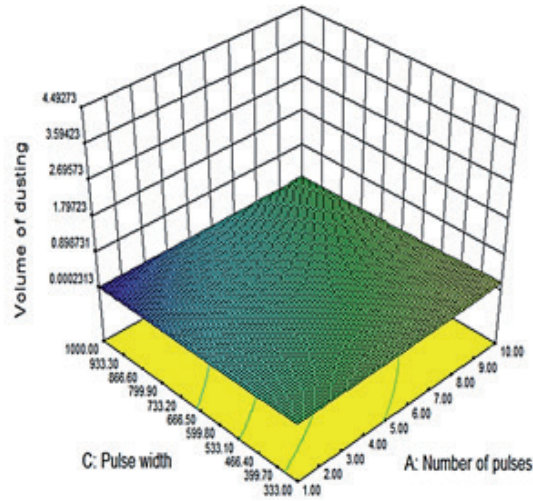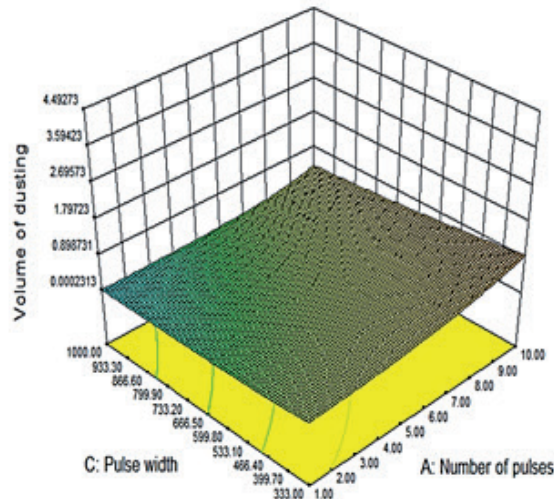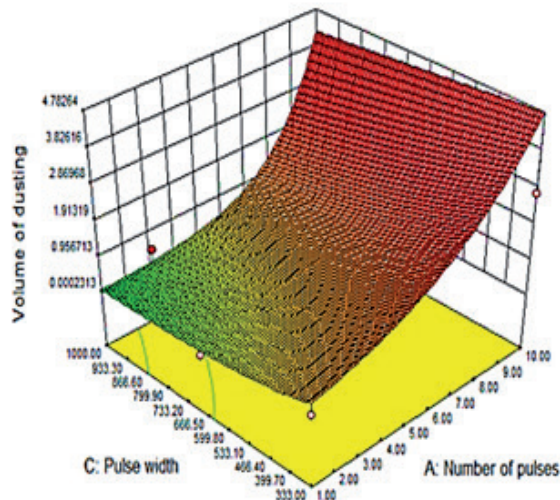
Figure 8.
The screenshots of the response surface of volume of ablation with two factors interactions fit against pulse width and the number of pulses at the pulse energy level of (a) 1 J; (b) 2 J; (c) 3 J.
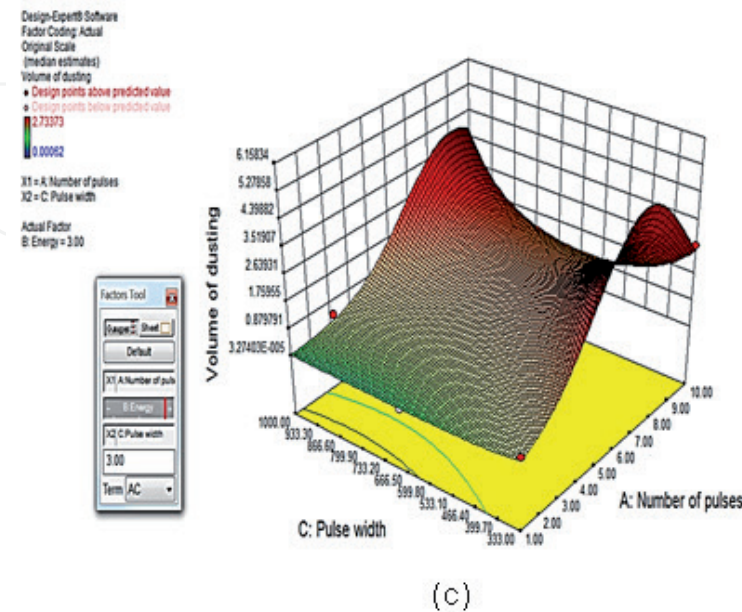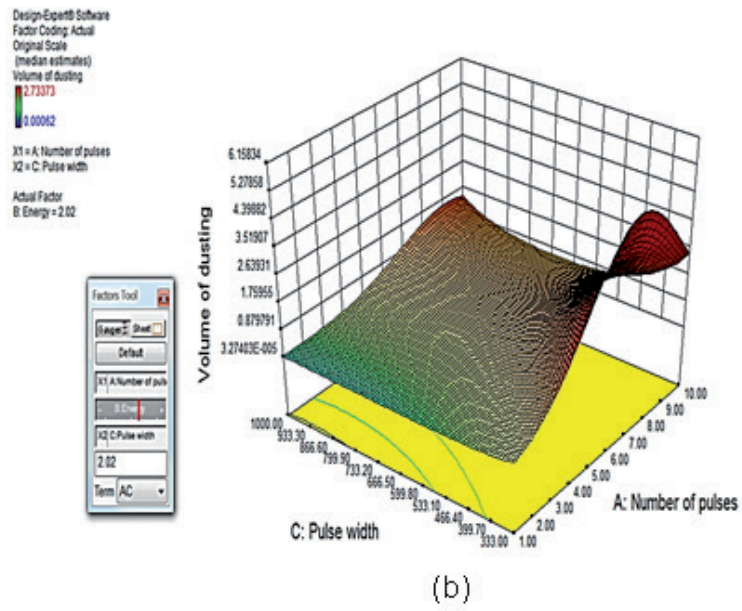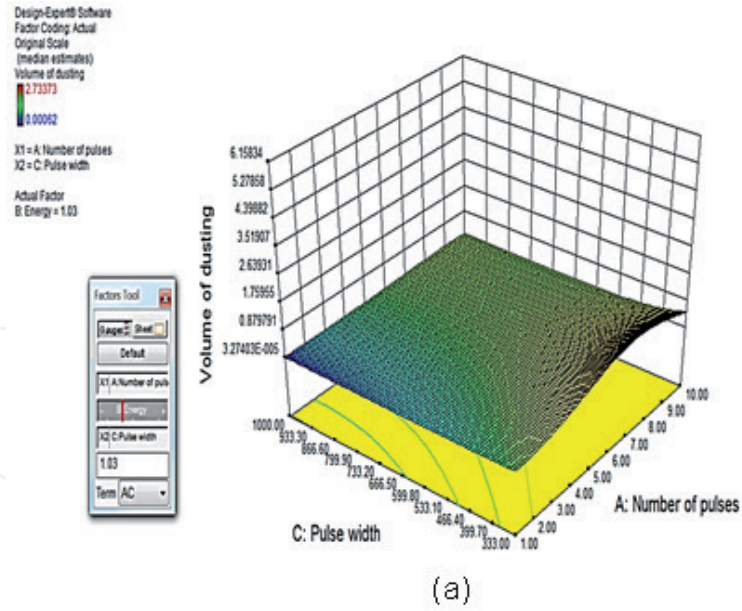
Figure 9.
The screenshots of the response surface of volume of ablation with quadratic fit against pulse width and the number of pulses at the pulse energy level of (a) 1 J; (b) 2 J; (c) 3 J.
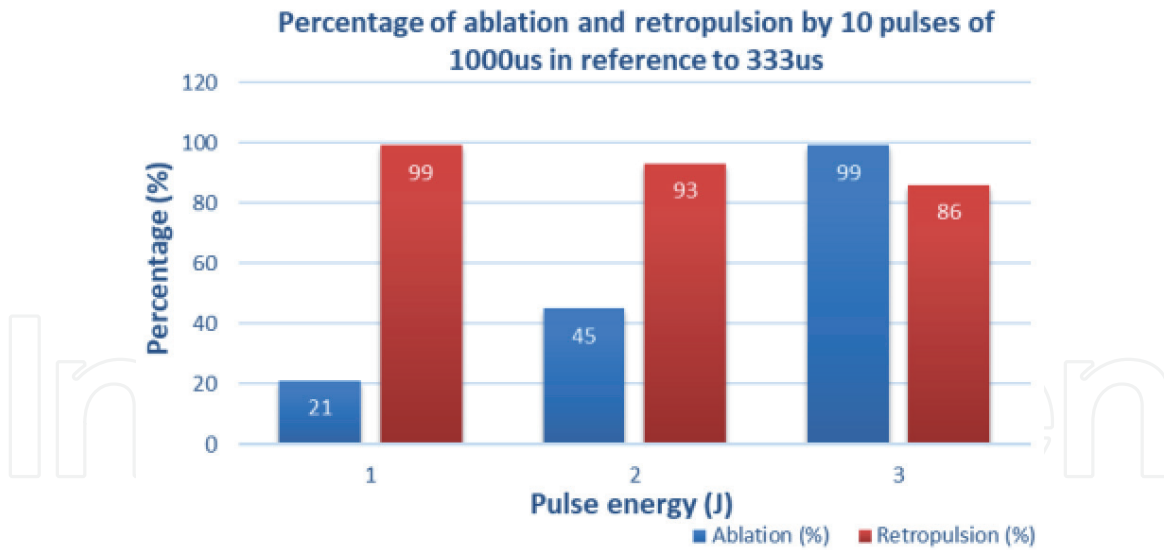
Figure 10.
The percentages of ablation and retropulsion by 10 pulses of the 1000 μs pulses in reference to those of 333 μs.
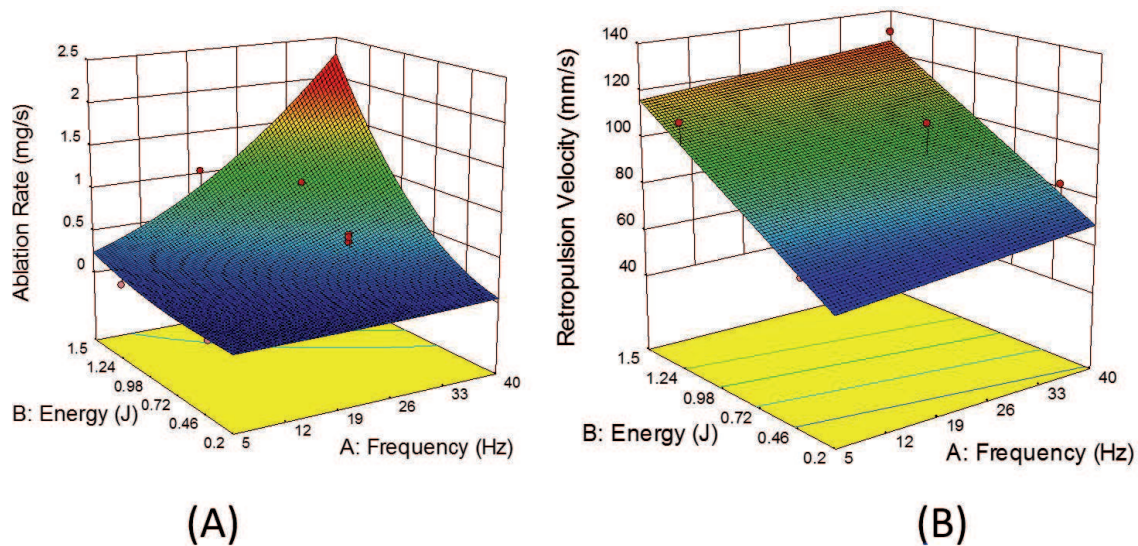

Figure 11.
(A) Response surface of ablation rate over laser pulse energy and frequency; (B) response surface of retropulsion velocity over laser pulse energy and frequency.

The actual analytical equation of ablation and retropulsion by laser pulse energy is:

$$A_{P-100}^{0.5} = -0.28 + 0.00064A + 0.41B + 0.015AB \qquad (6)$$

$$R_{P-100} = 49.1 + 0.28A + 43.8B \qquad (7)$$

Figure 12(A) and **(B)** are the optimized laser settings listed with equal weight ratio between ablation rate and retropulsion velocity. The 1st optimized laser setting is 1.2 J 40 Hz. IF we choose a 1:3 weight ratio between ablation rate and retropulsion velocity, the 1st optimized laser setting becomes 0.6 J 40 Hz. This means the "optimized" laser setting depends on the criterion used.
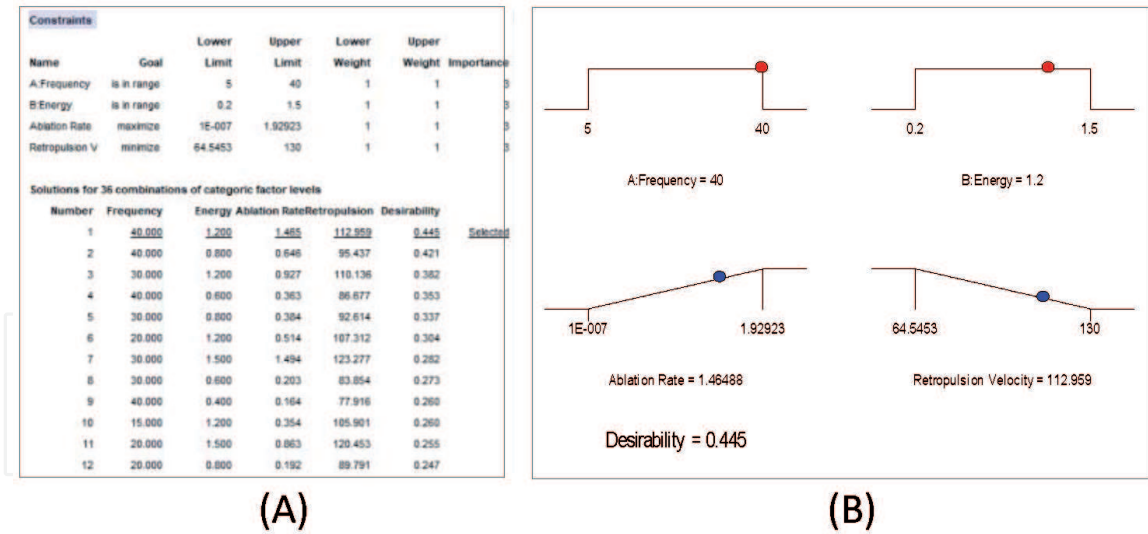
Figure 12.
(A) List of optimized laser parameters with even weight (50/50) of ablation and retropulsion speed; (B) ramp view of the chosen laser parameters with even weight (50/50) of ablation and retropulsion speed.
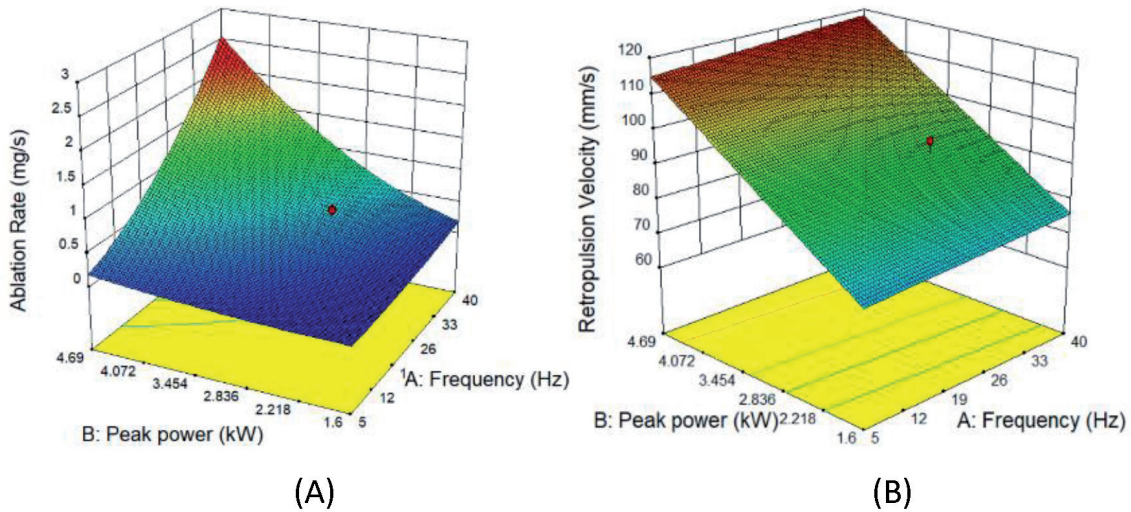

Figure 13.
(A) Response surface of ablation rate over laser pulse peak power and frequency; (B) response surface of retropulsion velocity over laser pulse peak power and frequency.

6.1.2 Response surface in terms of laser pulse peak power

The laser pulse peak power is another way of evaluating the laser damage to the stone [63]. The peak power value is defined by the laser pulse energy over the full pulse width (full width of pulse at ~10% of max amplitude). The ANOVA shows an insignificant lack of fit, acceptable agreement of the Predicted and Adjusted R-Squares, and acceptable precision (> 4.0).

Figure 13 (A) and **(B)** are the screenshots of the response surface of ablation rate and the retropulsion velocity in terms of laser pulse peak power.

Coded analytical equation of ablation and retropulsion by laser pulse Peak power is:

$$A_{P-100}{}^{0.5} = 0.60 + 0.41A + 0.40B + 0.19AB \tag{8}$$

$$R_{P-100} = 95.5 + 1.62A + 21.06B - 0.87AB \tag{9}$$
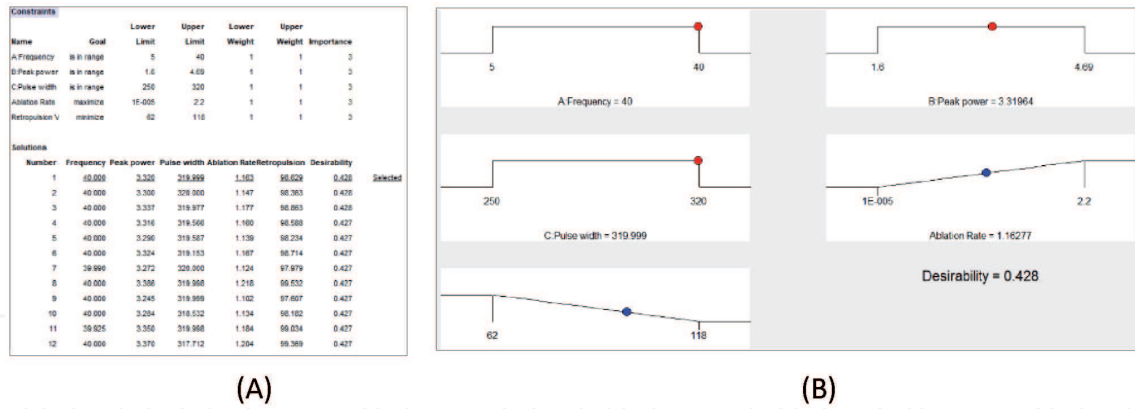
Figure 14.
(A) List of optimal laser settings with equal weight (50/50) of ablation rate and retropulsion velocity;
(B) ramp view of the selected laser settings with equal weight (50/50) of ablation rate and retropulsion velocity.

A_{P-100} is the Ablation rate, R_{P-100} is the Retropulsion speed, A is the Frequency, B is the Peak power, and C is the Pulse width.

From the Eqs. 8 and 9, we can see the peak power has roughly the same influence as the frequency on the ablation rate; and for retropulsion speed, the peak power's influence is 13 folds that of the frequency. Namely, the peak power parameter is crucial to retropulsion speed.

The actual analytical equation of ablation and retropulsion by laser pulse peak power is:

$$A_{P-100}{}^{0.5} = -0.26 + 0.0016A + 0.11B + 0.0069AB \qquad (10)$$

$$R_{P-100} = 57.6 + 0.093A + 13.6B - 0.025AB \qquad (11)$$

Figure 14(A) and **(B)** are the optimized laser settings listed with an equal weight ratio of the ablation rate and retropulsion velocity. The 1st optimized laser setting is 3.3 kW 40 Hz 320 μs. IF we choose a 1:3 weight ratio of the ablation rate and retropulsion velocity, the 1st optimized laser setting becomes 2.2 kW 40 Hz 320 μs. This means the "optimized" laser setting depends on the criterion used.

7. Discussion

7.1 The quantitative responses of calculus ablation and retropulsion in terms of the pulse energy, pulse width, and the number of pulses of a prototype CTH:YAG laser system

In the coded formulas of the response surface (1) and (2), the pulse energy is the dominant control input factor for both the responses of retropulsion and ablation (1.42 and 1.11); while the control input pulse width has more than an order of magnitude less influence on the responses of ablation and retropulsion (−0.0083 versus −0.0021). And the two-factor terms have even lesser influence (a few times to an order of magnitude) than the first-order terms. The pulse number term seems to have some nonlinear effects between long and short pulses at pulse numbers ~7-8 from **Figure 9**. This effect could be due to the vapor bubble behavior of [47]. As it is shown in **Figure 15(b)** since the vapor bubble of the long laser pulse will have a much-elongated shape bubble which
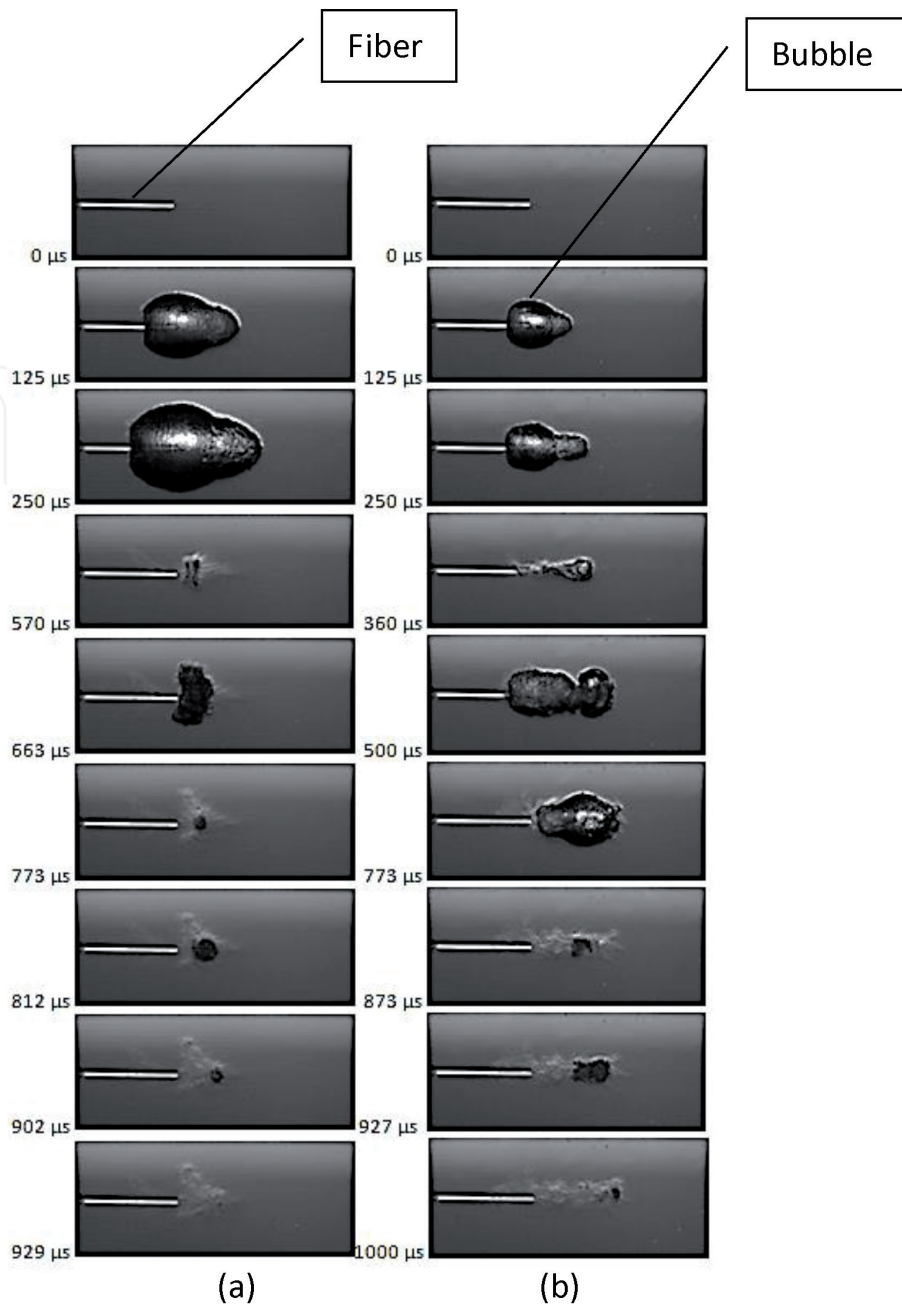
Figure 15.
Series of screenshots of vapor bubbles behavior of Ho lasers. (a) Ho at 1 J, 150 µs; (b) Ho at 1 J, 800 µs.

can be divided into two small bubbles which will collapse sequentially with the 2nd bubble collapses further away from the fiber tip as compared to the bubble of a short laser pulse. Therefore, the long laser pulse can make a deeper crater. This effect will be enhanced at higher pulse energy, and furthermore, since both fiber and calculus were fixed, the depth of the hole max out after ~7-8 pulses.

7.2 The laser setting optimization of laser lithotripsy of a commercially available CTH:YAG laser system

For the response of ablation rate, the coded formulas of the response surface reveal that the control input laser pulse energy is 1.4 times as impactful as that of the frequency, and the laser pulse peak power has the same impact as the frequency; while for the response of retropulsion, the control input laser pulse energy is 5.8 times as impactful as that of the frequency, and laser pulse peak power has 13 times

as impactful as the frequency. The laser pulse peak power is the dominant control input factor for the response of stone retropulsion during laser lithotripsy.

As for the optimal lithotripsy laser dosimetry (setting), there are conflict interests to deliver more energy per time (more power or fluence) and achieve faster lithotripsy but at the cost of more retropulsion and larger fragments. As concluded by Sea J et al. in Ref [47], the optimal lithotripsy laser setting depends on the individual case condition (calculus type, size, location, etc.) and the desired outcome. The response surfaces are generated by analysis of variance (ANOVA) of the tested data points, and a ranked list of the optimized laser settings can be generated by the criteria the user selected. If the least retropulsion is the desired, the most effectual method to curtail stone retropulsion during laser lithotripsy is to decrease the peak power (which has the maximum influential coefficient in the coded response surface equations). Dongyul C et al. investigated the ablation thresholds of stone sample by peak power density [63], which presents a recommendation of the lowest peak power for Bego calculus phantom ablation.

8. Conclusions

In this chapter, the application of RSM were conducted by two sets of DOE experiments: 1) with a prototype CTH:YAG laser system, the RSM reveals that the dominant control input laser parameters that influence the responses of lithotripsy outcome: the ablation or retropulsion is Inversely proportional to the pulse width, and the pulse width has a higher impact coefficient to the ablation than that to the retropulsion. The quadratic fit of the response surface for the volume of ablation has a nonlinear relationship with the pulse width and number of the pulse. 2) the laser setting optimization of laser lithotripsy of a commercially available CTH:YAG laser system: a series of laser settings for relatively efficient laser lithotripsy (maximize the ablation rate while minimizing the retropulsion as well as to improve the discharge of fragments via the urinary tract) in terms of control input laser pulse energy and peak power. Comparing to the control input frequency, the laser pulse energy or peak power has a higher impact coefficient to the response of stone retropulsion as compared to the response of stone ablation in Ho:YAG laser lithotripsy. The most efficient way to curtail stone retropulsion during laser lithotripsy is to lower the laser pulse peak power.

More detailed investigation of the optimal conditions for the ablation of other kinds of calculus samples and the fiber size/burn back effects will be conducted as a future study.

Acknowledgements

Disclaimer

The opinions expressed in this book chapter is solely those of the author and not necessarily those of Boston Scientific Corporation (BSC). BSC does not guarantee the accuracy or reliability of the information provided herein.

Author details

Jian J. Zhang
Boston Scientific Corporation, Marlborough, MA, USA

*Address all correspondence to: james.zhang@bsci.com

IntechOpen

References

[1] Yang C, Li S, Cui Y; "Comparison of YAG Laser Lithotripsy and Extracorporeal Shock Wave Lithotripsy in Treatment of Ureteral Calculi: A Meta-Analysis." Urol Int; 98:373-381 (2017).

[2] Bader MJ, Pongratz T, Khoder W, Stief CG, Herrmann T, Nagele U, Sroka R. Impact of pulse duration on Ho:YAG laser lithotripsy: fragmentation and dusting performance. World J Urol. 2015; 33: 471-477.

[3] Graham A, Luber S, Wolfson AB. Urolithiasis in the Emergency Department. Emerg. Med. Clin. North Am. 2011;29(3):519-538.

[4] Türk C, Neisius A, Petřík A, Seitz C, Thomas K, Skolarikos A. EAU guidelines on urolithiasis 2018. in European Association of Urology Guidelines. Presented at the EAU Annual Congress, Copenhagen., 2018th ed., The European Association of Urology Guidelines Office, Arnhem, The Netherlands 2018.

[5] Matlaga BR, Jansen JP, Meckley LM, Byrne TW, Lingeman JE. Economic outcomes of treatment for ureteral and renal stones: a systematic literature review. J. Urol. 2012;188(8):449-454.

[6] Rizvi SAH, Naqvi SAA, Hussain Z, Hashmi A, Hussain M, Zafar MN, Mehdi H, Khalid R. The management of stone disease. BJU Int. 2002;89(Suppl. 1):62-68.

[7] Tiselius HG. Epidemiology and medical management of stone disease. BJU Int. 2003; 91: 758-767.

[8] Scales CD. Jr. Practice Patterns in the Management of Urinary Lithiasis. Curr Urol Rep 2013; 14: 154-157.

[9] Turney BW, Reynard JM. The Cost of Stone Surgery. EUROPEAN UROLOGY 2014; 66: 730-731.

[10] Antonelli JA, Maalouf NM, Pearle MS, Lotan Y. Use of the National Health and Nutrition Examination Survey to calculate the impact of obesity and diabetes on cost and prevalence of urolithiasis in 2030. Eur Urol 2014; 66:724-729.

[11] Pearle MS, Calhoun EA, Curhan GC, Urologic Diseases of America Project. Urologic diseases in America project: urolithiasis. The Journal of Urology. 2005; 173(3): 848-857.

[12] Seklehner S, Laudano MA, del Pizzo J, Chughtai B, Lee RK. Renal calculi: trends in the utilization of shock-wave lithotripsy and ureteroscopy. The Canadian Journal of Urology. 2015; 22(1): 7627-7634.

[13] Maiman TH (1967) Ruby laser systems. US Patent 3,353,115.

[14] Mulvaney WP, Beck CW. The Laser Beam in Urology. J. Urol. 1968; 99: 112-115.

[15] Watson G, Smith N. Comparison of the pulsed dye and holmium lasers for stone fragmentation: in-vitro studies and clinical experience. Proceedings of SPIE. 1993; 1879: 139-142.

[16] Tischer C, Koort HJ, Bazo A, Rasch R, Thiede C. Clinical experiences with a new frequency-doubled doublepulse Nd:YAG laser (FREDDY) for the treatment of urolithiasis. Proceedings of SPIE, 2002; 4609: 128-135.

[17] Sayer J, Johnson DE, Price RE, Cromeens DM. Endoscopic laser fragmentation of ureteral calculi using the holmium:YAG. Proceedings of SPIE. 1993; 1879: 143-148.

[18] Grasso M, Chalik Y. Principles and applications of laser lithotripsy: experience with the holmium laser

Lithotrite. Journal of Clinical Laser Medicine & Surgery, 1998; 16(1): 3-7.

[19] Marguet CG, Sung JC, Springhart WP, L'esperance JO, Zhou SL, Zhong P, Albala DM, Preminger GM. In vitro comparison of stone retropulsion and fragmentation of the frequency doubled, double pulse Nd:YAG laser and the holmium:YAG laser. The Journal of Urology, 2005; 173(5): 1797-1800.

[20] Marks AJ, Teichman JMH. Lasers in clinical urology: state of the art and new horizons. World Journal of Urology. 2007; 25(3): 227-233.

[21] Jansen ED, van Leeuwen TG, Motamedi M, Borst C, Welch AJ. Temperature dependence of the absorption coefficient of water for midinfrared laser radiation. Lasers in Surgery and Medicine. 1994; 14(3): 258-268.

[22] Teichman JMH, Vassar GJ, Glickman RD. Holmium: yttrium-aluminum-garnet lithotripsy efficiency varies with stone composition. Urology. 1998; 52(3): 392-397.

[23] Grasso M. Experience with the holmium laser as an endoscopic lithotrite. Urology. 1996; 48(2): 199-206.

[24] Chan KF, Vassar GJ, Pfefer TJ. et al. Holmium:YAG laser lithotripsy: a dominant photothermal ablative mechanism with chemical decomposition of urinary calculi. Lasers in Surgery and Medicine. 1999; 25(1): 22-37.

[25] Pierre S, Preminger GM. Holmium laser for stone management. World Journal of Urology. 2007; 25(3): 235– 239.

[26] Teichman JMH, Rogenes VJ, McIver BJ, Harris JM. Holmium:yttrium-aluminum-garnet laser cystolithotripsy of large bladder calculi. Urology. 1997; 50(1): 44-48.

[27] Fried NM, Irby PB. Advances in laser technology and fiberoptic delivery systems in lithotripsy. Nat Rev Urol. 2018; 15: 563-573.

[28] Traxer O, Keller EX. Thulium fiber laser: the new player for kidney stone treatment? A comparison with Holmium:YAG laser. World Journal of Urology. 2019; Feb 06

[29] Frenz M, Zweig AD, Romano V, Weber HP. Dynamics in laser cutting of soft media. Proceedings of SPIE. 1990; 1202: 22-33

[30] Niemz M. Laser- Tissue Interactions – Fundamentals and Applications. 2nd Edition, 2002; pp72, Springer ISSN 1618-7210 ISBN 3-540-42763-5.

[31] Rajabhandharaks D, Zhang JJ, Wang H, Xuan JR, Chia RWJ, Hasenberg T, Kang HW. Dependence of water content in calculus phantom during Q-switched Tm:YAG laser lithotripsy. Proc. SPIE 8565, Photonic Therapeutics and Diagnostics IX, 2013; 856519.

[32] Rajabhandharaks D, Zhang JJ, Wang H, Xuan JR, Chia RWJ, Hasenberg T, Kang HW. Water content contribution in calculus phantomablation during Q-switched Tm:YAG laser lithotripsy. Journal of Biomedical Optics 2015; 20(12): 128001.

[33] Zhang JJ, Xuan JR, Yu H, Devincentis D. Study of cavitation bubble dynamics during Ho:YAG laser lithotripsy by high-speed camera. Proc. SPIE 9689, Photonic Therapeutics and Diagnostics XII, 2016: 1-7.

[34] Isner JM, Clarke RH. Cardiovascular Laser Therapy. Raven Press, New York. 1989.

[35] Chan KF, Pfefer TJ, Teichman JMH, Welch AJ. A Perspective on Laser Lithotripsy: The Fragmentation Processes. JOURNAL OF ENDOUROLOGY. 2001; 15(3): 257-273.

[36] Strittmatter F, Eisel M, Brinkmann R, Cordes J, Lange B, Sroka R. Laser-induced lithotripsy: a review, insight into laboratory work, and lessons learned. Translational Biophotonics, 2020; e201900029.

[37] Zhang JJ, Getzan G, Xuan JR, Yu H. Study of fiber-tip damage mechanism during Ho:YAG laser lithotripsy by high-speed camera and the Schlieren method. Proc. of SPIE. 9303 Photonic Therapeutics and Diagnostics XI, 2015; 930311-1-10.

[38] Lauterborn W, Vogel A. ShockWave Emission by Laser Generated Bubbles. Springer-Verlag, C.F. Delale (Ed.): Bubble Dynamics & Shock Waves, SHOCKWAVES 8, 2013: 67-103.

[39] Kuznetsov LI. Recoil momentum at a solid surface during developed laser ablation. Quantum Electronics. 1993; 23(12): 1035-1038.

[40] Foth HJ, Meyer D, Stockel T. Side effects of laser-tissue interaction studied by laser Doppler vibrometry. Proceedings of SPIE, 2000; 4072: 392-400.

[41] White MD, Moran ME, Calvano CJ, Borhan-Manesh AL, Mehlhaff BA. Evaluation of retropulsion caused by holmium: YAG laser with various power settings and fibers. Journal of Endourology. 1998; 12(2): 183-186.

[42] Lee HO, Ryan RT, Teichman JMH, et al. Stone retropulsion during holmium:YAG lithotripsy. The Journal of Urology. 2003; 169(3): 881-885.

[43] Lee H, Ryan RT, Kim JH, et al. Dependence of calculus retropulsion dynamics on fiber size and radiant exposure during ho:YAG lithotripsy. Journal of Biomechanical Engineering. 2004; 126(4): 506-515.

[44] Finley DS, Petersen J, Abdelshehid C, et al. Effect of holmium: YAG laser pulse width on lithotripsy retropulsion in vitro. Journal of Endourology. 2005; 19(8): 1041-1044.

[45] Scales CD Jr, Smith AC, Hanley JM, Saigal CS, and Urologic Diseases in America Project, "Prevalence of kidney stones in the United States," European Urology, vol. 62, no. 1, pp. 160-165, 2012.

[46] Jian J. Zhang; Jonathan Rutherford; Metasebya Solomon; Brian Cheng; Jason R. Xuan; Jason Gong; Honggang Yu; Michael Xia; Xirong Yang; Thomas Hasenberg; Sean Curran, "The study of laser pulse width on efficiency of Ho:YAG laser lithotripsy", Proc. SPIE 10038, Photonic Therapeutics and Diagnostics XIII, 1-7 (2017)

[47] D. S. Finley, J. Petersen, C. Abdelshehid et al., "Effect of holmium:YAG laser pulse width on lithotripsy retropulsion in vitro," Journal of Endourology, vol. 19, no. 8, pp. 1041-1044, 2005.

[48] Spore SS, Teichman JMH, CorbinNS, ChampionPC, WilliamsonEA, Glickman RD. Holmium:YAG lithotripsy: optimal power settings. Journal of Endourology. 1999; 13(8): 559-566.

[49] Sea J, Jonat LM, Chew BH, et al. Optimal power settings for holmium:YAG lithotripsy. The Journal of Urology. 2012; 187(3): 914-919.

[50] Teichman JMH, Rao R, Glickman R, Harris J. Holmium:YAG percutaneous nephrolithotomy: the laser incident angle matters. The Journal of Urology. 1998; 159(3): 690-694.

[51] Vassar GJ, Teichman JMH, Glickman RD. Holmium:YAG lithotripsy efficiency varies with energy density. The Journal of Urology. 1998; 160(2): 471-476.

[52] Kang HW, Lee H, Teichman JMH, Oh J, Kim J, Welch AJ. Dependence of

calculus retropulsion on pulse duration during ho: YAG laser lithotripsy. Lasers in Surgery and Medicine. 2006; 38(8): 762-772.

[53] Deters LA, Pais VM Jr. Difference in Operative Time According to Stone Location for Endoscopic Management of Ureteral and Renal Stones. Urology. 2013; 81(3): 522-526.

[54] Carey RI, Kyle CC, Carey DL, and Leveillee RJ. "Preparation of artificial kidney stones of reproducible size, shape, and mass by precision injection molding," J Endourol 2008; 22(1), 127-131.

[55] Eisel M, Strobl S, Pongratz T, Strittmatter F, Sroka R. Holmium:yttrium-aluminum-garnet laser induced lithotripsy: in-vitro investigations on fragmentation, dusting, propulsion and fluorescence. Biomed. Opt. Express 2018; 9(11): 5115.

[56] Eisel M, Strobl S, Pongratz T, Strittmatter F, Sroka R. In vitro investigations of propulsion during laser lithotripsy using video tracking. Lasers Surg. Med. 2018; 50: 333-339.

[57] Zhang JJ, Rajabhandharaks D, Xuan RJ, Chia RWJ, Hasenberg TC. Characterization of Calculus Migration during Ho:YAG Laser Lithotripsy by High Speed Camera Using Suspended Pendulum Method. Proc. SPIE 8926, Photonic Therapeutics and Diagnostics X, 2014; 89261I-1-7.

[58] Kronenberg P, Traxer O. Update on lasers in urology 2014: current assessment on holmium:yttrium–aluminum–garnet (Ho:YAG) laser lithotripter settings and laser fibers. World J. Urol. 2015; 33: 463-469.

[59] T. C. Hutchens, D. A. Gonzalez, P. B. Irby, N. M. Fried, Fiber optic muzzle brake tip for reducing fiber burnback and stone retropulsion during thulium fiber laser lithotripsyJ. Biomed. Opt. 2017; 22(1): 18001.

[60] Sroka R, Haseke N, Pongratz T, Hecht V, Tilki D, Stief CG, Bader MJ. In Vitro Investigations of Repulsion During Laser Lithotripsy Using a Pendulum Setup. Lasers Med. Sci. 2012; 27: 637.

[61] Zhang JJ, Rajabhandharaks D, Xuan R J, Chia RWJ, Hasenberg TC. Calculus migration characterization during Ho:YAG laser lithotripsy by high-speed camera using suspended pendulum method. Lasers Med. Sci. 2017; 32: 1017-1021.

[62] Esch E, Simmons WN, Sankin G, Cocks HF, Preminger GM, Zhong P. A simple method for fabricating artificial kidney stones of different physical properties. Urol Res. 2010; 38(4): 315-319.

[63] Chai DY, Zhang JJ, Podana N, Xuan RJ, Hasenberg T, Harrah T. The study of Ho: YAG laser ablation thresholds of calculus phantom in terms of peak power density. Proc. SPIE 10852, Therapeutics and Diagnostics in Urology 2019; 108520D.